FT-RAMAN, XRD AND DIELECTRIC STUDIES ON HUMAN

GALLSTONES IN PUDUCHERRY REGION

R. VIJAYAPRASATH<sup>1</sup>, R. SELVARAJU<sup>2</sup>

<sup>1</sup>Department of Physics, Manakula Vinayagar Institute of Technology, Puducherry 605 107.

2. Engineering Physics, Faculty of Engineering and Technology, Annamalai University,

Annamalainagar 608 002.

**ABSTRACT** 

Biocrystallization, a vital process in living organisms, facilitates the formation of highly

structured minerals within biological tissues, enabling the creation of superior materials such

as teeth, bones, and shells. This interdisciplinary field encompasses biology, chemistry,

physics, and materials science. While beneficial processes like bone mineralization are

essential for health, pathological biocrystallization, such as that seen in gallstone disease

(cholelithiasis), poses significant health risks, leading to organ dysfunction and various clinical

complications. This study focuses on understanding the molecular mechanisms underlying

gallstone formation by analyzing cholesterol supersaturation dynamics, crystal formation, and

bile composition. The investigation aims to characterize the chemical and mineral composition

of gallstones, utilizing techniques such as Fourier Transform-Raman spectroscopy and X-ray

diffraction to explore their dielectric properties for potential diagnostic applications

Keywords: Gallbladder, FT-Raman, XRD, Dielectric loss

1. INTRODUCTION

Biocrystallization is the process through which living organisms direct the formation

of finely structured minerals within their tissues. To regulate inorganic components and arrange

them into beautifully organized crystalline structures, organisms require complex biological control systems. This process is referred to as "biocrystallization" because it specifically involves biological guidance that protects these highly ordered and functional crystal structures [1]. Teeth, bones, and shells, which often possess superior properties compared to their humanmade counterparts. Biocrystallization has emerged as a crucial interdisciplinary field that integrates biology, chemistry, physics, and materials science. Unlike abiotic crystallization, which is governed by thermodynamic equilibrium, biologically controlled crystal formation occurs within complex cellular environments and is kinetically regulated [2]. Living systems can produce crystals with remarkable structural complexity, intricate layered structures, and specific functional properties[3]. In contrast to beneficial processes like bone mineralization, pathological biocrystallization involves abnormal crystal formation within the body, which poses a serious health risk[4]. This detrimental crystallization can lead to organ malfunction, tissue damage, and debilitating clinical symptoms. Millions of people worldwide suffer from cholelithiasis, commonly known as gallstone disease, which is one of the most prevalent gastrointestinal disorders. Solid deposit mostly made of cholesterol buildup inside the gallbladder as a result of this illness[5]. Biliary supersaturation and consequent stone formation are caused by a combination of pathophysiological, nutritional, hormonal, metabolic and heredity variables[1,5]. In addition to being extremely common, cholelithiasis is clinically significant as a leading cause of morbidity and medical costs worldwide. Acute cholecystitis, biliary colic, gallstone pancreatitis, choledocholithiasis and cholangitis are among the problems that might result from cholelithiasis symptoms [7]. To understand the molecular mechanism underlying gallstone disease a thorough analysis of the dynamics of cholesterol supersaturation, crystal formation and bile composition is required. Recent advancements in bile microstructural research have improved our understanding of the early phases of gallstone formation. Cholesterol Supersaturation Index (CSI)". The cholesterol saturation index (CSI) is

a crucial physicochemical metric that determines the probability of gallstone development [8]. Although cholesterol levels remain the same, patients with gallstone have 33% and 31% lower levels of phospholipids and bile acids, respectively, compared to healthy individuals" [10]. In the biliary tree, gallstone are solid aggregates composed of protein aggregates, calcium and cholesterol monohydrate crystals. The physical properties of mature gallstones are determined by the crystalline structure of cholesterol monohydrate[]. Gallstone disease (GSD) is a worldwide health burden with a complicated and multidimensional etiology. According to current epidemiology research, gallstone development is caused by a variety of risk factors, such as metabolic illness, lifestyle variables and demographic features. India's gallstones epidemiology shows notable regional differences in North India, the prevalence of symptomatic gallstone is 20 times greater than in South India, one of the most noticeable differences in the world [11]. Over the past ten years, notable regional disparities in occurrence have surfaced. The burden is greater in the northern areas, which is consistent with Delhi startlingly high gallbladder cancer incidence rate of 21.5 per 100,000 females which is among the highest in the world []. In line with worldwide gender distribution trends, population-based studies conducted in the rural Gangetic basin of North India show a 4.15% overall gallstone prevalence with a noticeable female preponderance (5.59% vs. 1.99% in men) [12].

Gathering gallbladder stones from gallstone patients and determining their chemical and mineral makeup are the goals of the current investigation. In order to test the stone's dielectric properties for diagnostic purposes, the dielectric loss and dielectric constant are calculated using the gathered stone's dielectric characteristics. The Fourier Transformer - Raman spectroscopy is used to find the chemical bonding and structure of the collected stones. The mineral composition of the stones is identified by X-ray diffractometer.

#### 2. MATERIALS AND METHOD

## 2.1 CLINICAL SURVEY ON GALLBLADDER STONE PATIENTS AND STONE COLLECTION

Patient's Stones in and around the Pondicherry Region. Gallstone were were collected from the patient and the collected specimens were gently washed with distilled water after collection. In order to prevent thermal exposure from changing the stones composition they were then allowed to air dry fully at ambient temperature. After dying the stones were placed in sterile containers, such as plastic vials or specimen containers: very tiny specimens were placed on filter paper. Patient identification, the date of collection and patient clinical features were carefully recorded for every sample. No chemical or preservatives were added, as these could compromise analytical accuracy. Each type of stone had a total of 10 samples gathered. Clinical information such as patient age, gender, stone position and size, history of recurrence, lifestyle variables (such as smoking and alcohol use) and dietary preferences (vegetarian and non-vegetarian) were gathered for the study. Microsoft Excel was used to analyze and graphically depict the data.

### 2.2 SAMPLING COLLECTED STONES

The collected 10 samples were divided into two groups based on the physical properties given in table 1.1. The group I gallbladder stones is codes as G1-G5 shown in Figure 1. and the Group II gallbladder stones are coded as G6-G10. Figure 1.2.



Fig 1.1 Human Gallbladder Stones Group I (G1-G5) (Light Gray Colour)



Fig 1.2 Human Gallbladder Stones Group II (G6-G10) (Brown Colour)

Table 1.1 Physical properties of human Gallbladder stone

Parameters	Group I	Group II
Colour	Light Gray	Light Brown
Size	1-1.5 cm	1-2 cm
Weight	0.985-7.706 gram	0.437-5.182 gram
Appearance	Granules	Oval and spherical
Surface	Rough	Semi polished
Cross section	Different layer form	Shiny crystalline nature
Hardness	Hard	Hard and Soft

### 3. RESULT AND DISCUSSION

## 3.1 X-RAY DIFFRACTION STUDIES ON GALLBLADDER STONES

The purpose of the X-ray diffraction (XRD) examination of human gallstones was to determine the interplanar spacing (d-spacing) and diffraction angle  $(2\theta)$ , as well as to match the chemical name with the JCPDS number (G1-G10).

## 3.1.1 X-RAY DIFFRACTION ANALYSIS OF GROUP I GALLBLADDER STONE (G1-G5)

The figures (3.1 – 3.5) illustrate the X-ray diffraction (XRD) spectra of gallbladder stones from Group I (G1 – G5). The analysis of the G1 sample reveals an initial phase of cholesterol (JCPDS 00-007-0742), characterized by prominent, well-defined peaks indicating a high degree of crystallinity. This suggests that cholesterol acts as an organic matrix within a biomineralized or composite material. Although minor differences in peak locations (0.01 to 0.5 degrees) arise from sample-specific variances, the close match with reference data ensures accurate phase identification. Table 3.1 presents the standard and observed values of G1 sample. Table 3.2 details the presence, quantity, and purity of calcium carbonate and cholesterol in the G2 samples. A thorough phase analysis reveals high-intensity peaks at 20.03 degrees and 21.15 degrees [13].

The G3 sample shows two main crystalline phases: calcium carbonate (JCPDS 00-009-0432) and cholesterol (JCPDS 00-007-0742). The purity of the cholesterol phase is confirmed by low-angle diffraction peaks close to 20.1 degrees, 20.7 degrees, 22.7 degrees, and 24.4 degrees [14]. Peaks in the mid-to-high-angle ranges indicate the presence of calcium carbonate, a significant biomineral. Results for these findings are displayed in Table 3.3, where the strong presence of cholesterol peaks confirms it as the primary organic component.

Table 3.4 presents the XRD spectrum data for the G4 sample, which indicates the presence of both calcium carbonate and crystalline cholesterol. The distinctive cholesterol peaks, referenced in JCPDS Card No: 00-007-0432, closely match diffraction peaks at 21.15 degrees, 23.5 degrees, and 24.7 degrees 2theta. Additionally, calcium carbonate is represented by peaks at 43.805 degrees, 44.3 degrees, and 53.14 degrees (JCPDS Card No: 00-009-0432)[13,14,17]. Table 3.5 presents the XRD results for the G5 sample, which reveals a complex combination of crystalline cholesterol. The presence of cholesterol indicates the

existence of an organic matrix, supporting the mineralization associated with the formation of gallbladder stones [15,16]. Figures 3.6 to 3.10 display the X-ray diffraction spectra of group II (G6-G10) gallbladder stones, while Tables 3.6 to 3.10 provide the standard and observed values, respectively.

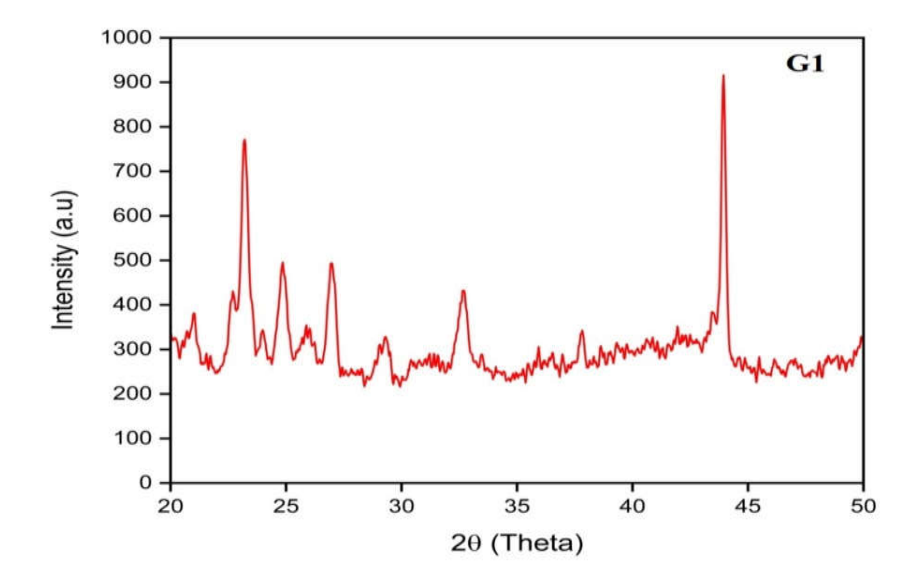


Fig 3.1 XRD spectrum of Group – I gallbladder stone sample (G1)

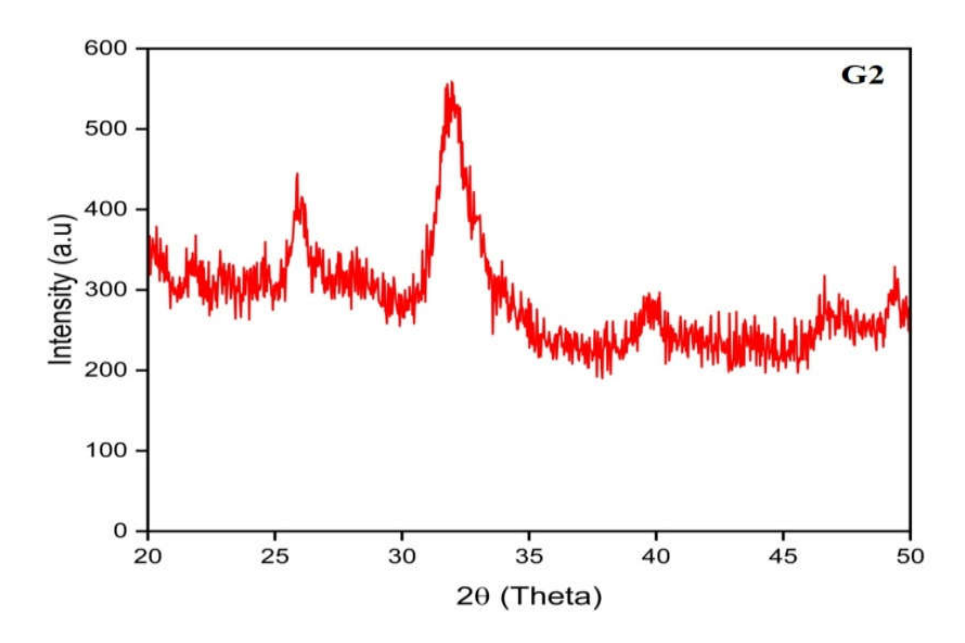


Fig 3.2 XRD spectrum of Group – I gallbladder stone sample (G2)

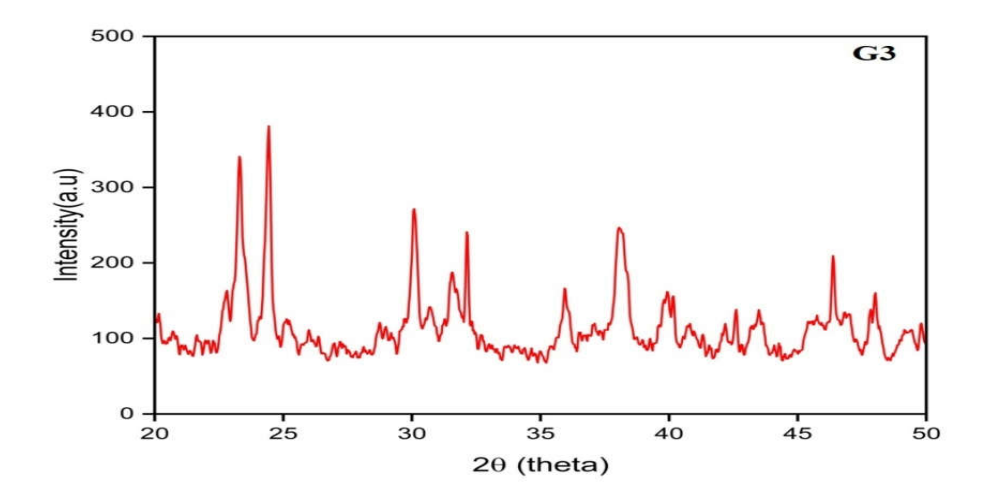


Fig 3.3 XRD spectrum of Group – I gallbladder stone sample (G3)

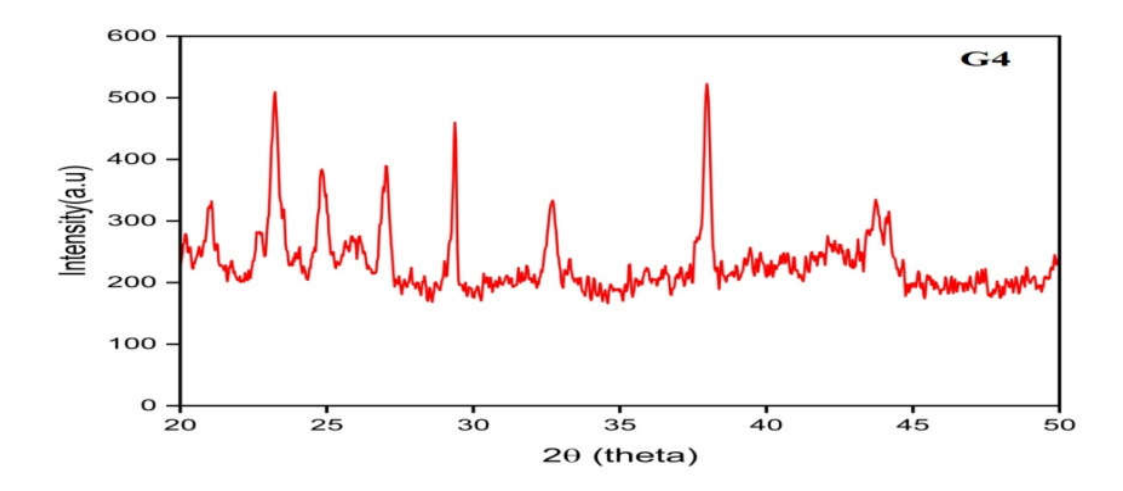


Fig 3.4 XRD spectrum of Group – I gallbladder stone sample (G4)

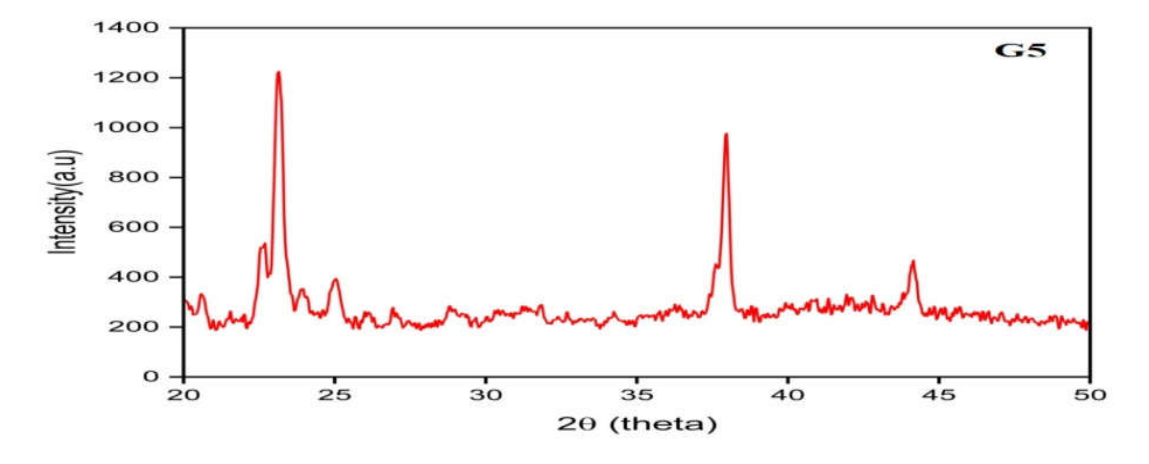


Fig 3.5 XRD spectrum of Group – I gallbladder stone sample (G5)

Table 3.1 Comparison between standard value and observed values of 2θ and d- spacing value of Group I gallbladder stone sample- (G1)

Standar	d values	Observed	values	7.070.0
2 theta	d[Å]	2 theta	d[Å]	JCPDS number
20.97	4.231	20.935	4.238	00-007-0742
22.67	3.916	22.724	3.908	00-007-0742
23.27	3.816	23.517	3.778	00-007-0742
23.96	3.709	23.517	3.778	00-007-0742
24.82	3.581	24.780	3.588	00-007-0742
25.95	3.428	25.879	3.438	01-086-2343
26.90	3.309	27.163	3.278	01-080-1793
29.32	3.042	29.416	3.032	01-080-1793
32.64	2.739	32.902	2.718	01-086-2343
35.97	2.493	35.481	2.527	01-086-2343
37.86	2.373	37.093	2.420	01-080-1793
41.87	2.154	41.321	2.182	01-080-1793
43.91	2.059	43.805	2.064	01-086-2343
45.42	1.994	45.306	1.999	01-086-2343

Table 3.2 Comparison between standard value and observed values of 2θ and d- spacing value of Group I gallbladder stone sample - (G2)

Standard v	Standard values		Observed values	
2 theta	d[Å]	2 theta	d[Å]	JCPDS number
20.28	4.373	20.03	4.426	01-080-1793
21.79	4.073	21.15	4.194	01-080-1793
25.97	3.425	25.87	3.438	01-080-1793
32.06	2.787	32.19	2.776	01-080-1793
42.38	2.129	42.31	2.133	01-080-1793
46.93	1.933	46.71	1.942	01-080-1793

Table 3.3 Comparison between standard value and observed values of  $2\theta$  and d- spacing value of Group I gallbladder stone sample- (G3)

Standard	Standard values		d values	LCDDC
2 theta	d[Å]	2 theta	d[Å]	JCPDS number
20.10	4.411	20.93	4.238	00-007-0742
20.70	4.284	20.93	4.238	00-007-0742
22.75	3.903	22.72	3.908	00-007-0742
23.32	3.809	23.51	3.778	00-007-0742
24.41	3.641	24.78	3.588	00-007-0742
25.16	3.534	25.87	3.438	01-086-2343
30.09	2.966	30.71	2.907	00-007-0742
31.59	2.828	31.77	2.812	00-007-0742
32.14	2.781	32.90	2.718	00-007-0742
35.96	2.493	35.48	2.527	01-086-2343
38.12	2.357	38.19	2.353	00-007-0742
39.93	2.254	39.67	2.268	00-007-0742
42.43	2.127	42.31	2.133	00-007-0742
43.45	2.080	43.80	2.064	00-007-0742
46.35	1.956	46.71	1.942	00-007-0742
47.97	1.893	47.79	1.900	00-007-0742

Table 3.4 Comparison between standard value and observed values of  $2\theta$  and d- spacing value of Group I gallbladder stone sample- (G4)

Standard	l values	Observed values		LCDDC
2 theta	d[Å]	2 theta	d[Å]	JCPDS number
21.01	4.223	21.15	4.194	00-007-0742
23.23	3.823	23.51	3.778	00-007-0742
24.86	3.577	24.78	3.588	00-007-0742
29.35	3.038	29.41	3.032	00-007-0742
32.67	2.737	32.19	2.776	00-007-0742
37.96	2.367	37.09	2.420	00-007-0742
37.96	2.367	37.09	2.420	00-007-0742
41.33	2.181	41.32	2.182	00-007-0742
43.726	2.067	43.80	2.064	01-086-2343
44.17	2.047	44.37	2.039	01-086-2343
53.14	1.721	53.14	1.721	01-086-2343

Table 3.5 Comparison between standard value and observed values of  $2\theta$  and d- spacing value of Group I gallbladder stone sample- (G5)

Standard	l values	Observed	l values	ICDDCl
2 theta	d[Å]	2 theta	d[Å]	JCPDS number
20.46	4.334	20.93	4.238	00-007-0742
22.62	3.924	22.72	3.908	00-007-0742
23.13	3.839	23.51	3.778	00-007-0742
23.82	3.730	23.51	3.778	00-007-0742
24.99	3.558	24.78	3.588	00-007-0742
28.75	3.100	28.96	3.078	01-086-2343
31.89	2.802	31.77	2.812	00-007-0742
33.71	2.655	33.98	2.634	00-007-0742
37.95	2.368	37.09	2.420	00-007-0742
44.11	2.050	44.37	2.039	01-086-2343

# 3.1.2 X-RAY DIFFFRACTION ANALYSIS OF GROUP I GALLBLADDER STONE (G6-G10)

The figures (3.6 - 3.10) illustrate the X-ray diffraction (XRD) spectra of gallbladder stones from Group II (G6 – G10). The G6 sample shows the presence of calcium carbonate (JCPDS 01-086-2343) and cholesterol (JCPDS 00-007-0742). Key diffraction peaks corresponding to the crystalline cholesterol phase are observed at 23.3 degrees and 24.8 degrees. Additionally, a peak around 29.4 degrees suggests mineral content linked to calcium carbonate [7]. This combination of inorganic calcium carbonate and organic cholesterol indicates a biomineralized substance. The G7 sample offers comprehensive phase identification based on both standard and observed diffraction characteristics. Cholesterol (JCPDS No. 00-007-0742) is responsible for most of the strongest peaks at low theta values (20 to 24 degrees), suggesting that it is the main organic component with high crystallinity. Calcium carbonate is represented by peaks around 25 degrees, 32 degrees, 36 degrees, and 43 degrees (JCPDS No. 00-009-0432) [14,16]. The G8 sample exhibits a composite character, showing both calcium carbonate (JCPDS 01-086-2343) and cholesterol (JCPDS 00-007-0742). Notable diffraction peaks between 20.6 degrees and 23.2 degrees indicate excellent crystallinity [18]. The calcium carbonate phase is also represented by several peaks in the mid-angle range, with only minor discrepancies between the standard and observed values. The G9 sample reveals a complicated composite nature that includes cholesterol (JCPDS 00-007-0742). Crystalline cholesterol is responsible for the major peaks at low values (around 23 degrees and 27 degrees)[15,17]. In the G10 sample, two primary crystalline phases—calcium carbonate and cholesterol—are observed. The predominant presence of cholesterol is confirmed by peaks that align with its JCPDS number 00-007-0742, particularly prominent between 20 degrees and 25 degrees in the 2theta range. An additional peak at 36 degrees may represent different crystal formations (polymorphic forms). Peaks near 32 degrees and 43 degrees correspond to calcium carbonate (JCPDS number 01-086-2343), indicating a mineral content of physiological significance [9,

13-16,19]. The exceptional crystallinity of this sample is crucial for understanding the material characteristics of this complex mixture.

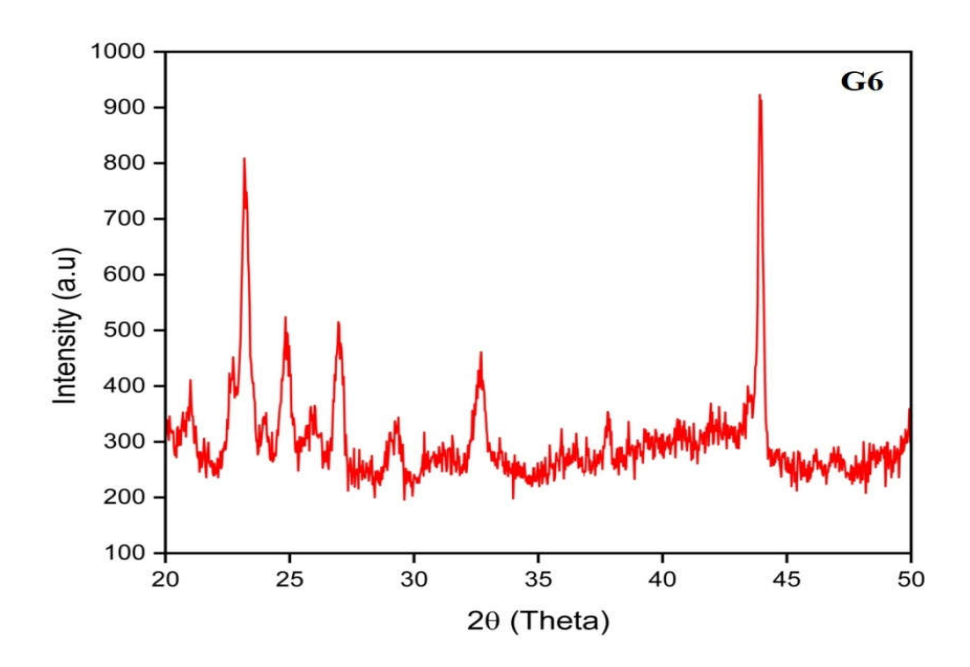


Fig 3.6 XRD spectrum of Group – II gallbladder stone sample (G6)

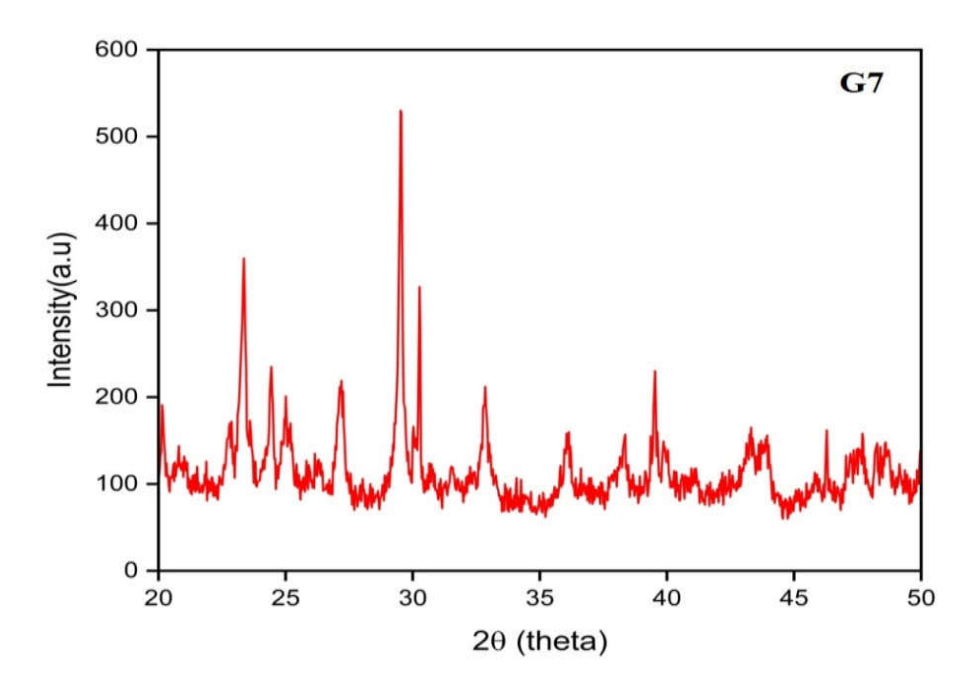


Fig 3.7 XRD spectrum of Group – II gallbladder stone sample (G7)

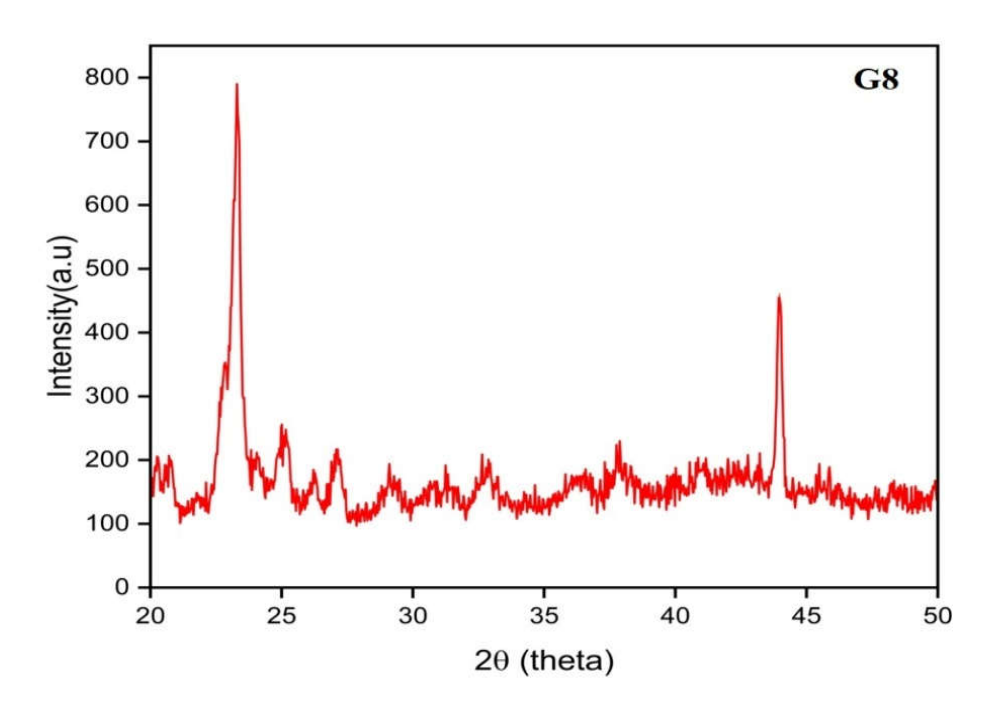


Fig 3.8 XRD spectrum of Group – II gallbladder stone sample (G8)

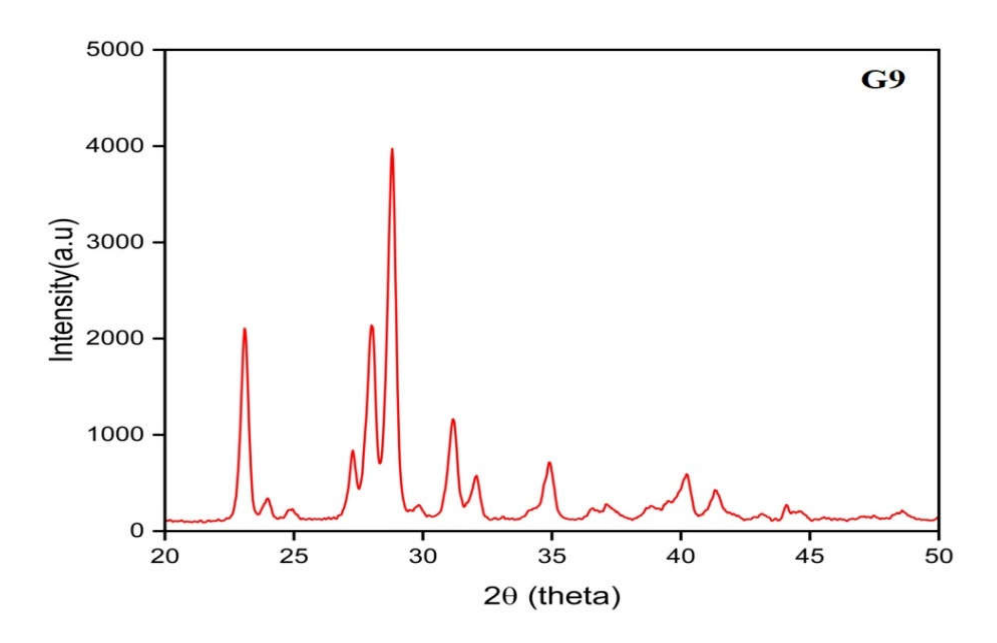


Fig 3.9 XRD spectrum of Group – II gallbladder stone sample (G9)

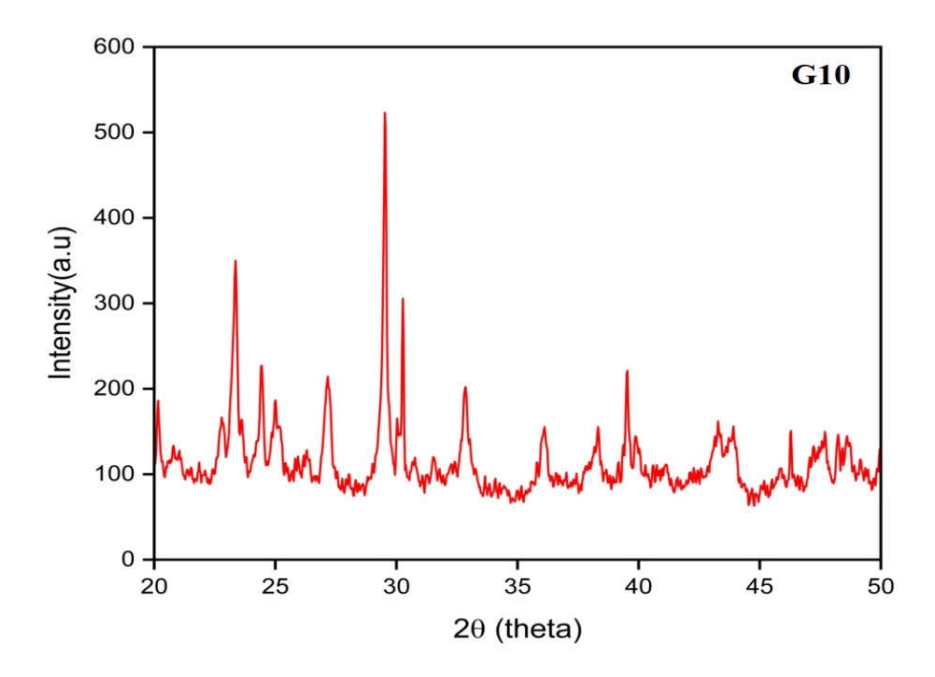


Fig 3.10 XRD spectrum of Group – II gallbladder stone sample (G10)

Table 3.6 Comparison between standard value and observed values of  $2\theta$  and d- spacing value of Group II gallbladder stone sample- (G6)

Standard va	Standard values Observed values		ICDDC assessible as	
2 theta	d[Å]	2 theta	d[Å]	JCPDS number
21.04	4.216	21.15	4.194	00-007-0742
23.31	3.810	23.51	3.778	00-007-0742
24.82	3.581	24.78	3.588	00-007-0742
29.24	3.049	29.41	3.032	01-086-2343
32.68	2.736	32.19	2.776	00-007-0742

Table 3.7 Comparison between standard value and observed values of  $2\theta$  and d- spacing value of Group II gallbladder stone sample - (G7)

Standa	rd values	Observed	values	JCPDS number
2 theta	d[Å]	2 theta	d[Å]	
23.33	3.807	23.51	3.778	00-007-0742
20.16	4.398	20.93	4.238	00-007-0742
22.79	3.896	22.72	3.908	00-007-0742
24.42	3.640	24.78	3.588	00-007-0742
25.03	3.553	25.87	3.438	01-086-2343
27.15	3.279	27.16	3.278	00-007-0742
29.52	3.022	29.41	3.032	00-007-0742
30.26	2.949	30.71	2.907	00-007-0742
32.84	2.723	32.19	2.776	01-086-2343
36.08	2.485	36.07	2.487	01-086-2343
39.52	2.277	39.67	2.268	00-007-0742
43.48	2.078	43.80	2.064	01-086-2343
46.27	1.959	46.71	1.942	01-086-2343

Table 3.8 Comparison between standard value and observed values of  $2\theta$  and d- spacing value of Group II gallbladder stone sample- (G8)

Standard valu	es	Observed	values	ICDDC assessibles
2 theta	d[Å]	2 theta	d[Å]	- JCPDS number
20.62	4.300	20.93	4.238	00-007-0742
23.24	3.822	23.51	3.778	00-007-0742
25.01	3.555	25.87	3.438	01-086-2343
27.09	3.287	27.16	3.278	00-007-0742
29.02	3.073	29.41	3.0327	00-007-0742
31.29	2.855	31.77	2.812	01-086-2343
32.57	2.745	32.90	2.359	01-086-2343
37.86	2.373	37.09	2.420	00-007-0742
43.23	2.090	43.80	2.064	01-086-2343
43.91	2.059	43.80	2.064	01-086-2343
45.46	1.992	45.30	1.999	01-086-2343
45.88	1.975	45.30	1.999	01-086-2343

Table 3.9 Comparison between standard value and observed values of  $2\theta$  and d- spacing value of Group II gallbladder stone sample- (G9)

Standard	values	Observed	values	JCPDS number
2 theta	d[Å]	2 theta	d[Å]	
23.09	3.847	23.51	3.778	00-007-0742
27.28	3.264	27.16	3.278	01-080-1793
28.00	3.1826	28.96	3.078	01-086-2343
23.94	3.711	23.51	3.778	00-007-0742
28.78	3.097	28.96	3.078	01-086-2343
31.15	2.867	31.77	2.812	01-086-2343
32.02	2.791	32.19	2.776	01-086-2343
34.87	2.569	34.87	2.569	01-080-1793
37.05	2.422	37.09	2.420	01-080-1793
40.07	2.247	40.45	2.227	01-086-2343
41.35	2.1806	41.32	2.182	01-080-1793
44.10	2.050	44.37	2.039	01-086-2343
48.55	1.872	48.62	1.870	01-086-2343

Table 3.10 Comparison between standard value and observed values of 2θ and d- spacing value of Group II gallbladder stone sample- (G10)

Standar	d values	Observed	values	ICDDC 1
2 theta	d[Å]	2 theta	d[Å]	JCPDS number
20.16	4.398	20.93	4.238	00-007-0742
23.33	3.808	23.51	3.778	00-007-0742
24.42	3.640	24.78	3.588	00-007-0742
25.03	3.552	25.87	3.438	00-007-0742
27.15	3.279	27.16	3.278	01-080-1793
29.52	3.022	29.41	3.032	01-080-1793
30.26	2.949	30.71	2.907	01-080-1793
32.84	2.723	32.90	2.718	01-086-2343
36.08	2.485	36.07	2.487	00-007-0742
38.27	2.349	38.19	2.353	00-007-0742
39.52	2.277	39.67	2.268	00-007-0742
43.25	2.089	43.80	2.064	01-086-2343
43.80	2.064	43.80	2.064	01-086-2343

## 3.2 FOURIER TRANSFORM-RAMAN SPECTROSCOPIC ANALYSIS OF GALLBLADDER STONES

# 3.2.1 FT-RAMAN SPECTRAL STUDIES ON GROUP I GALLBLADDER STONES (G1-G5)

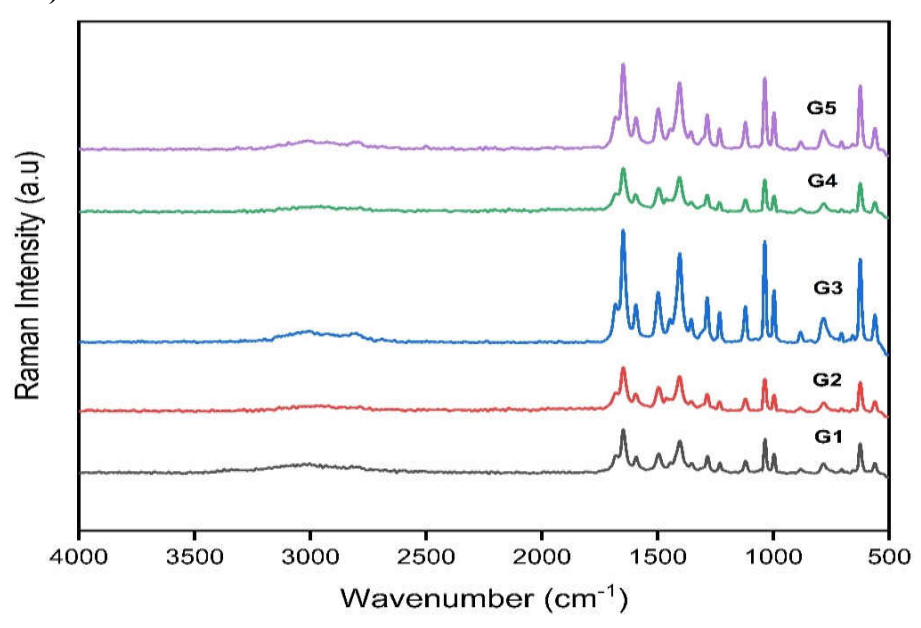


Fig 3.11 FT- Raman spectrum of Group – I gallbladder stone sample - (G1 – G5)

A complete set of Raman shift spectrum data for gallstone samples G1 through G5 seen in Figure 3.11, is given in Table 3.11. The anticipated functional groups and backbone structure of cholesterol are confirmed by the existence of distinctive O-H, CH<sub>2</sub>, C=C, and skeletal vibrations. Sample purity, hydrogen bonding conditions, or physical states may alter based on slight variations in peak locations extending vibrations from O-H (3333 to 3110 cm<sup>-1</sup>). The hydroxyl group (-OH) found in cholesterol molecules is characterized by O-H stretching in samples, which ranges from around 3003 cm<sup>-1</sup> to 3012 cm<sup>-1</sup> [20]. The wavenumber variation suggests that the hydroxyl group is being affected by variations in the environment or hydrogen bonding. CH<sub>2</sub> Stretching (1352-1496 cm<sup>-1</sup>): Symmetric and Asymmetric Features. 1648 cm<sup>-1</sup> C=O Ring Stretching The sterol ring system's strong characteristic peaks validate the cholesterol core structure, which includes the ring's unsaturated bonds. Displacement of G3 (1400 to 1500 cm<sup>-1</sup>). This vibration mode involves C-O ring stretching vibration mode (ROH)-chol suggestive is observed at 1231 cm<sup>-1</sup>. C-C Skeletal Stretching and Bending (782 to 895;

703 cm<sup>-1</sup> and lower) [20,21,22]. Bands in these regions report on the carbon-carbon backbone's vibrational modes including bending and stretching within the molecular skeleton. C-H bending vibration is seen near 700 cm<sup>-1</sup>. The weak band at 783, 04, 562 are assigned to presence of C-O bending, Po<sub>4</sub><sup>3-</sup> bending and skeletal Ring deformation. The strongest vibration mode of peak at 625 is due to ring breathing mode [23].

Table 3.11 FT-Raman absorption frequencies (cm<sup>-1</sup>) estimate along with tentative assignment for Group – I gallbladder stones - (G1-G5)

	Wavenumber (cm <sup>-1</sup> )			Tentative assignment	
G1	G2	G3	G4	G5	
3003	3288	3007	3288	3012	O-H Stretching vibration (Hydroxyl)
-	2954	-	2954	2812	CH <sub>2</sub> symmetric stretching vibration
1648	1648	1648	1648	1648	C=O stretching vibration
1592	1594	1593	1594	1593	C=C stretching
1496	1495	1497	1495	1497	C-H deformations
1404	1405	1404	1405	1405	CH <sub>2</sub> stretching
1352	1355	1354	1355	1356	CH <sub>2</sub> stretching
1284	1286	1286	1286	1286	C-O stretching
1231	1233	1232	-	1232	C-O stretching
1120	1120	1121	-	1120	C=C stretching
1036	1037	1037	1037	1037	C-C-H plane bending
997	997	997	997	997	CH <sub>2</sub> Wagging
881	883	882	883	881	CaCo <sub>3</sub> bending
783	782	782	-	784	C-O bending CaCo <sub>3</sub>
704	705	706	705	705	Po <sub>4</sub> <sup>3-</sup> bending vibration
625	624	625	624	625	Ring breathing mode
561	562	561	562	561	Skeletal ring deformation

## 3.2.2 FT-RAMAN SPECTRAL STUDIES ON GROUP II GALLBLADDER STONES (G6 – G10)

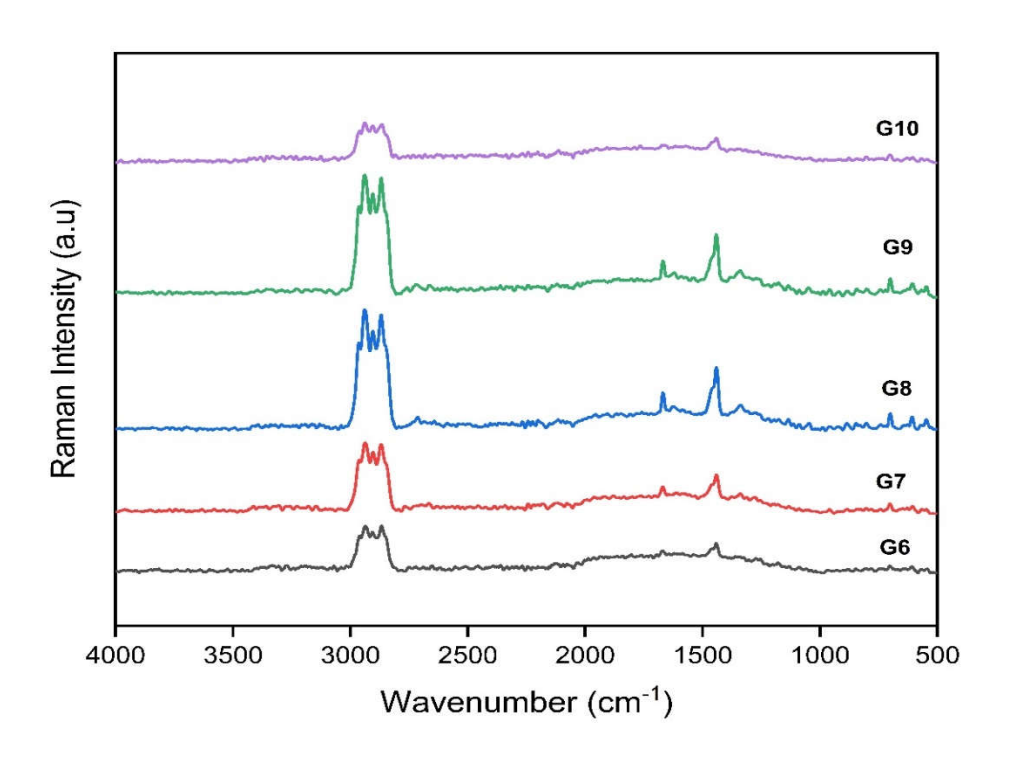


Fig 3.12 FT- Raman spectrum of Group – II gallbladder stone sample- (G6- G10)

The gallbladder samples from G6 to G10 are listed in Table 4.2.2 along with comprehensive "Raman shift spectral" data. All of these details describe the vibration spectra, which are shown in figure 3.12. For the G6, G7, and CH 10 samples, the O-H stretching vibrations are detected around 3300-3340. This is a hydroxyl group absorption characteristic. This indicates differences in the hydrogen's or its model environment's bonding. The stretching vibration of CH2 at 2868-2935 cm<sup>-1</sup> are symmetric and asymmetric [17,20,21]. However, it represents the methylene groups found in the fat's hydrocarbon chains. In G9 and G8, the out-of-plane C-H bending vibration was detected at 2702 and 2713 cm<sup>-1</sup>. From 1605 to 1670 cm<sup>-1</sup>, the C=O ring stretch vibrates [23,24]. This provides more evidence that oxygen is functioning. The CH2 stretching vibrations are located between 1338 and 1339 cm<sup>-1</sup>. It has been determined that the PO<sub>4</sub><sup>3-</sup> bending vibrations are between 606 and 703 cm<sup>-1</sup>.

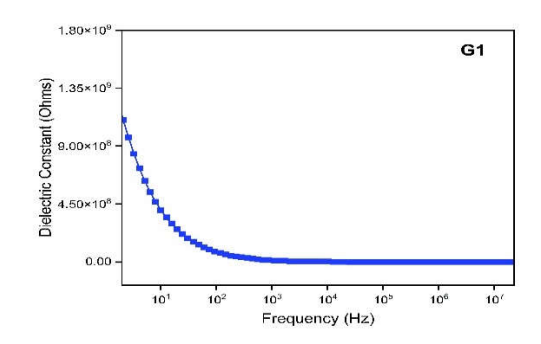
Table 3.12 FT-Raman absorption frequencies (cm<sup>-1</sup>) estimate along with tentative assignment for Group – II gallbladder stones (G6- G10)

Wavenumber (cm <sup>-1</sup> )					Tentative assignment
G6	G7	G8	G9	G10	Tentative assignment
3333	3305	-	-	3383	O-H Stretching vibration
2935	2936	2938	2939	2938	CH <sub>2</sub> symmetric stretching vibration
-	2903	2904	2904	2904	CH <sub>2</sub> asymmetric stretching vibration of CH <sub>3</sub>
2867	2868	2869	2868	2866	CH <sub>2</sub> and CH <sub>3</sub> symmetric stretching vibration
-	-	2713	2702	-	C-H asymmetric stretching of CH <sub>2</sub>
2124	2117	-	-	2113	N-H stretching
1670	1669	1668	1668	1664	C-C stretching
1442	1440	1441	1441	1441	CH <sub>2</sub> stretching
-	1339	1338	1338	-	CH <sub>2</sub> Wagging
703	702	701	700	701	Po <sub>4</sub> <sup>3-</sup> bending vibration
-	606	608	606	-	Po <sub>4</sub> <sup>3-</sup> bending vibration

### 3.3 DIELECTRIC STUDIES ON GALLBLADDER STONE

Dielectric measurements were performed to examine the electrical properties of human gallstones (labeled G1 to G10) across a range of frequencies. We analyzed how the dielectric parameters varied with frequency to gain insights into the polarization mechanisms, charge distribution, and the impact of the stones' chemical composition on their electrical properties.

### 3.3.1 DIELECTRIC STUDIES ON GROUP I GALLBLADDER STONES



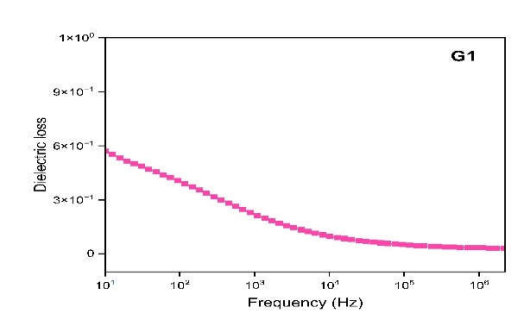
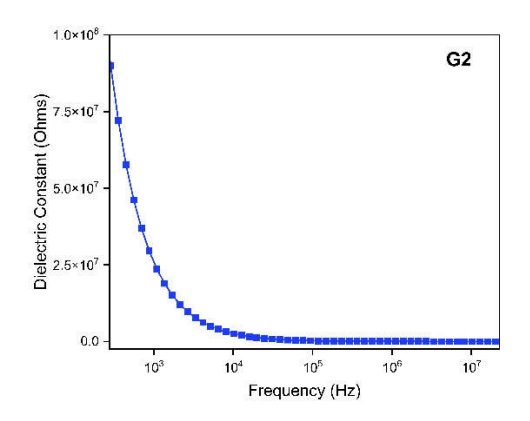


Fig 3.13 Dielectric analysis of Group I gallbladder stone sample - (G1)
(a)Dielectric constant (b) Dielectric loss



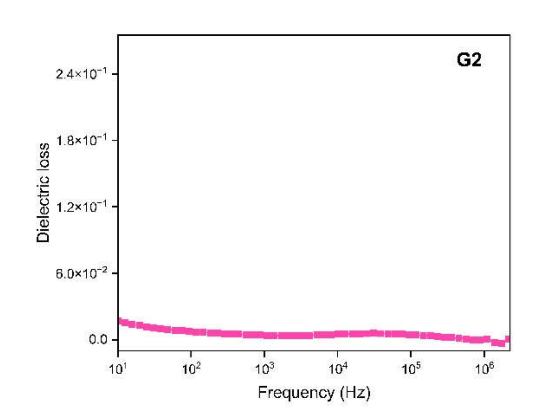
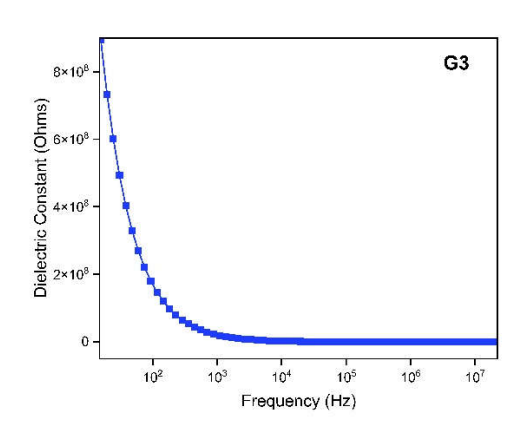


Fig 3.14 Dielectric analysis of Group I gallbladder stone sample – (G2)
(a) Dielectric constant (b) Dielectric loss



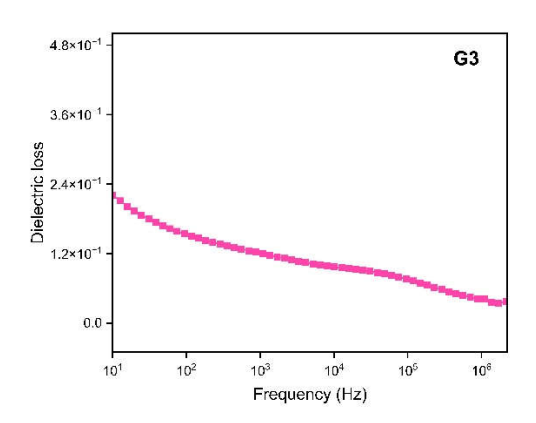
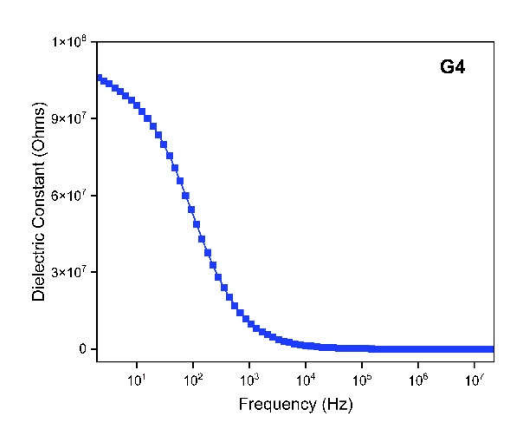


Fig 3.15 Dielectric analysis of Group I gallbladder stone sample – (G3)
(a) Dielectric constant (b) Dielectric loss



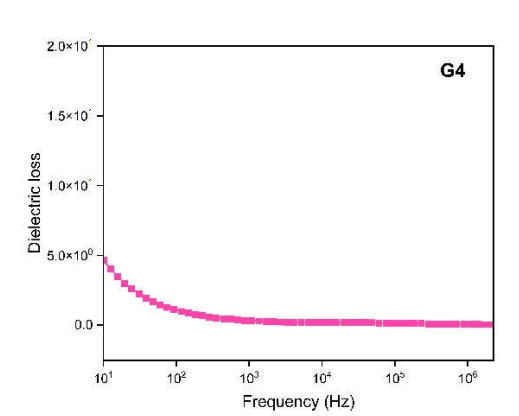
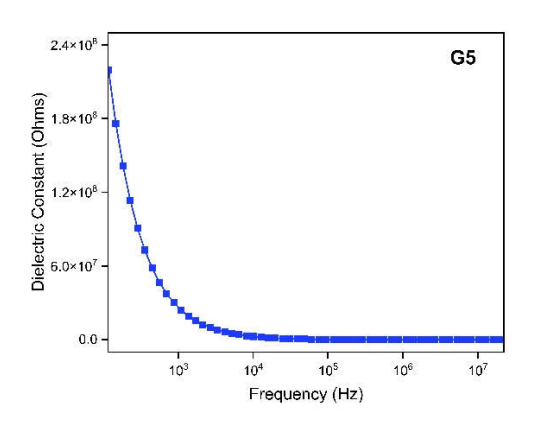


Fig 3.16 Dielectric analysis of Group 1 gallbladder stone sample – (G4)
(a) Dielectric constant (b) Dielectric loss



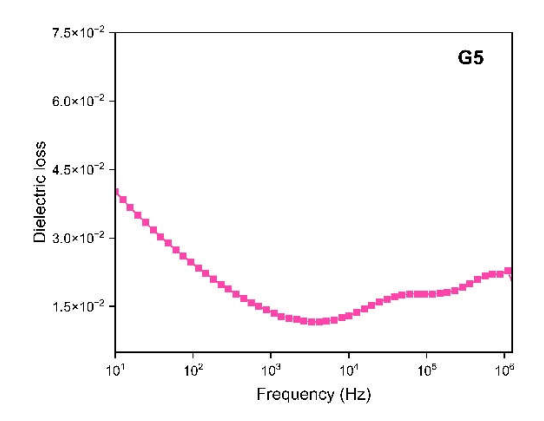


Fig 3.17 Dielectric analysis of Group I gallbladder stone sample – (G5)
(a) Dielectric constant (b) Dielectric loss

Figures 3.13 (a) to 3.17(a) demonstrate the distinctive dielectric spectra displayed by the sample (G1, G2, G3, G4 and G5). At low frequencies, the G1 sample has the largest dielectric constant, measuring about  $1.7 \times 10^9$  Ohms, G2 on the other hand, displays the lowest values, at about  $1 \times 10^8$  Ohms. The notable variation implies that the polarisation capabilities of these samples are influenced by different material compositions, microstructures, or preparation techniques.

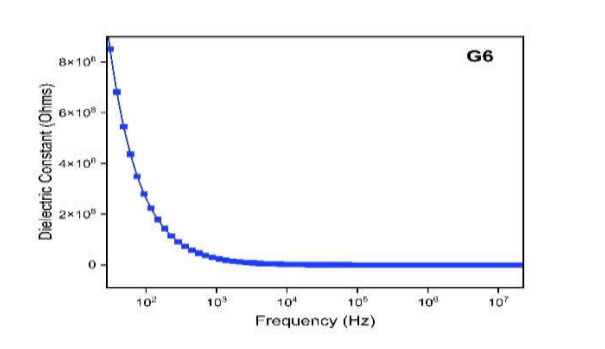
The frequency response patterns show that the dielectric constant is significantly reduced in all samples in the low to mid-frequency region, usually between 1 Hz and 10<sup>4</sup> Hz. After about 10<sup>4</sup> Hz, all sample's dielectric constants stabilize at low values [26]. The sample dispersion curves vary in steepness; G3 and G5 show abrupt transitions, whilst G1 and G4 which might be connected to the samples various charge carrier types or structural heterogeneity levels.

Figures 3.13 (b) to 3.17 (b) show the samples from G1 through G5 exhibiting normal insulating behavior, where dielectric loss reduces with increasing frequency. This is consistent with the basic idea that dipoles cannot keep up with the fast-changing electric field at high frequencies, which results in less energy being dissipated. Dielectric loss and frequency often exhibit a power-law connection in the graphs, which is especially noticeable in the low to mid-frequency region (1 Hz to  $\sim 10^3$  Hz).[27,28]

This shows that dielectric relaxation has the form  $\epsilon$ "  $\propto$  f(-n), where for the majority of insulating materials, n usually falls between 0.5 and 1.5. At low frequencies, G4 has the largest

dielectric loss values, reaching about  $1.8 \times 10^{-2}$ , respectively, G3 shows intermediate loss levels (about  $4.5 \times 10^{-1}$ ).

### 3.3.2 DIELECTRIC STUDIES ON GROUP II GALLBLADDER STONES (G6-G10)



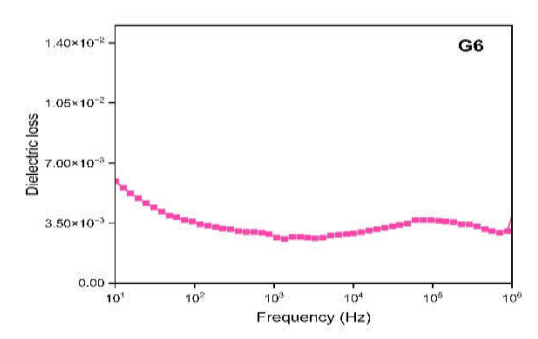
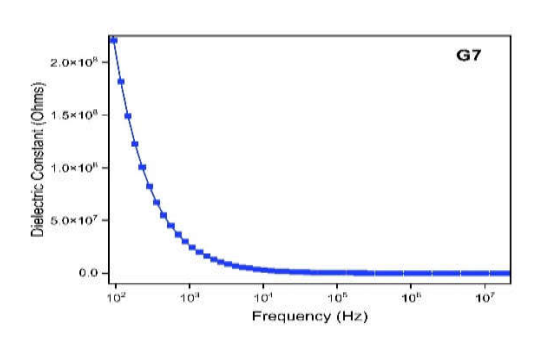


Fig 3.18 Dielectric analysis of Group II gallbladder stone sample – (G6)
(a) Dielectric constant (b) Dielectric loss



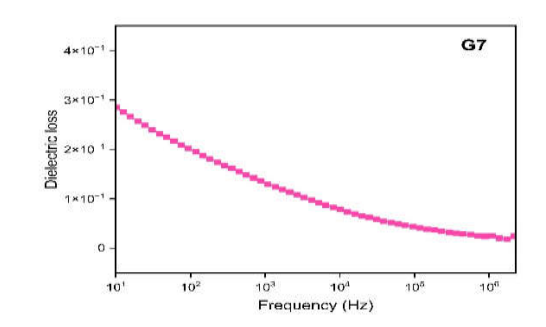
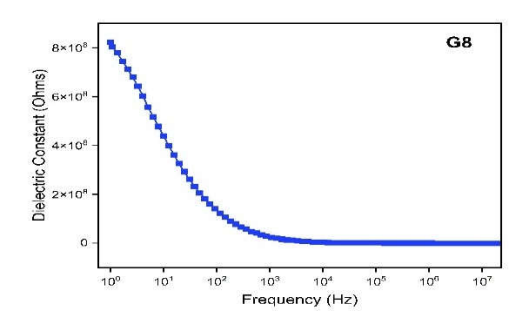


Fig 3.19 Dielectric analysis of Group II gallbladder stone sample – (G7)
(a) Dielectric constant (b) Dielectric loss



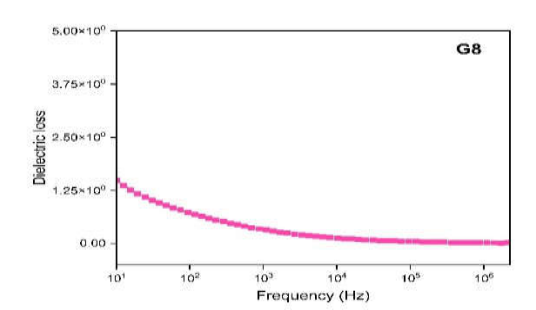
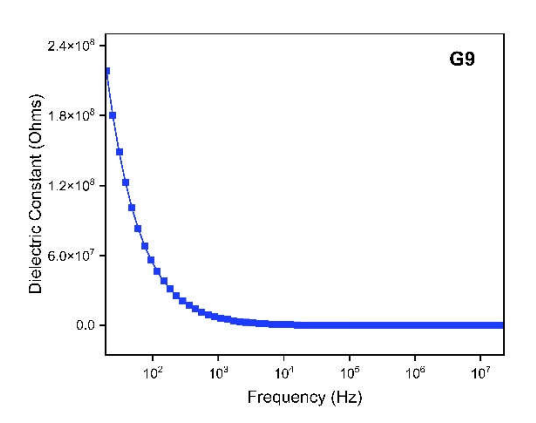


Fig 3.20 Dielectric analysis of Group II gallbladder stone sample – (G8) (a) Dielectric constant (b) Dielectric loss



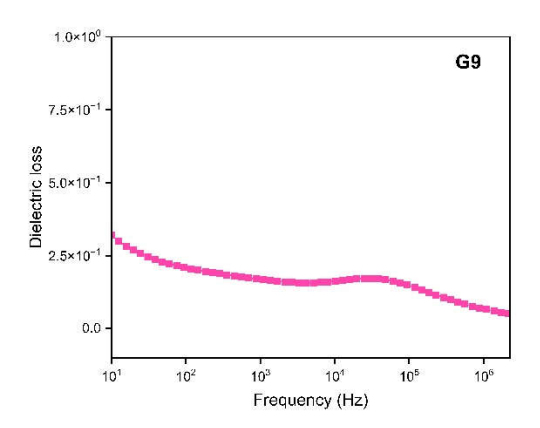
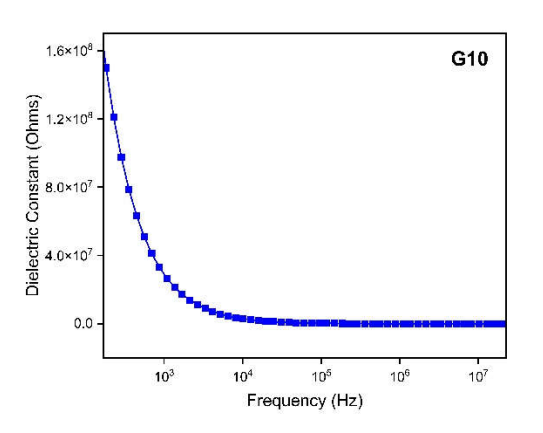


Fig 3.21 Dielectric analysis of Group II gallbladder stone sample – (G9)
(a) Dielectric constant (b) Dielectric loss



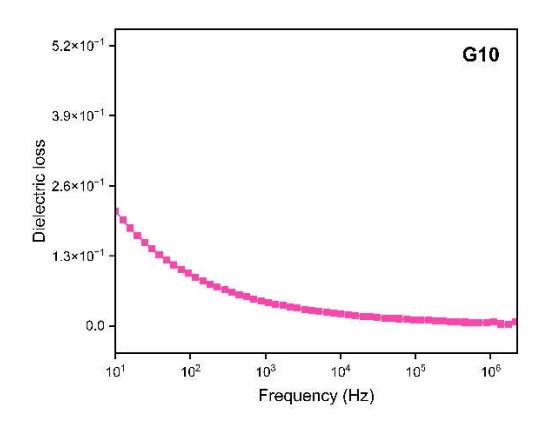


Fig 3.22 Dielectric analysis of Group II gallbladder stone sample – (G10)
(a) Dielectric constant (b) Dielectric loss

Figures 3.18 (a) to 3.22(a) illustrate the dielectric dispersion pattern of the sample (G6, G7, G8, G9, and G10), which is typical of materials having strong interfacial polarisation or Maxwell-Wagner relaxation effects. All samples reach a low, roughly zero dielectric constant value at frequencies higher than  $10^4$  to  $10^5$  Hz. This implies that there is a minimum dielectric response at high frequencies because the polarisation processes are unable to keep up with the changing electric field. The dielectric constant values exhibit a rapid rise at lower frequencies, suggesting the existence of interfacial polarization effects. This type of behaviour is common is heterogeneous materials where charge buildup takes place at electrode-sample or phase contacts. Of all the samples, G6 had the most modest response, with a maximum dielectric constant of around  $9 \times 10^8$  Ohms. Although its total magnitude is rather smaller, its dispersion

starts, and G7 exhibits a maximum frequency rise, the curve exhibits a smooth transition. G8 behaves similarly however, its maximal dielectric constant is somewhat lower at about  $8 \times 10^8$  Ohms. Its frequency range allows for a more thorough understanding of the dispersion behaviour by extending to lower frequencies (beginning at  $10^0$  Hz). G10 and G9 exhibit the most noticeable low-frequency dispersion; at the lowest measured frequencies, their dielectric constants were around  $1.6 \times 10^8$  Ohms, respectively [28].

Considering the two samples, the behaviour shifts from high to low frequencies at about  $10^3$  Hz. These materials most likely have conductive phases or show notable interfacial effects, based of the observed behaviour. Usually, electrode polarisation or space charge effects – where charges build up at interfaces and are difficult to dissipate at low frequencies – are linked to the sharp increase in dielectric constant at low frequencies. In contrast to actual dielectric polarisation, this leads to an apparent high dielectric constant that is more strongly associated with conductivity effects. [27,28]

Figures 3.18(b) to 3.22(b) illustrate how the dielectric loss behaviour of samples from G6 to G10 changes with frequency. The lowest total dielectric loss values are found in G6, which starts at roughly  $1.05 \times 10^{-2}$  at 1 Hz and drops to about  $3 \times 10^{-3}$  at  $10^6$  Hz. Interestingly, the loss marginally increases at higher frequencies (>10<sup>5</sup> Hz), suggesting the emergence of additional polarisation mechanisms. G7 has modest loss values, with a smooth decline devoid of notable aberrations, beginning at  $4 \times 10^{-1}$  at 1 Hz and gradually declining to ground  $2 \times 10^{-2}$  to  $10^6$  Hz.

The sample with the largest dielectric loss, G8, reaches over 4.5 at 1 Hz and drops almost to conductivity. G9 exhibits intermediate behaviour, exhibiting a particular relaxation process, with a minor plateau in the mid-frequency band (10<sup>2</sup>-10<sup>4</sup> Hz) and a decrease from 0.85 at 1 Hz to 0.05 at 10<sup>6</sup> Hz. G10 has a standard relaxation pattern devoid of characteristics, starting at 1 Hz with a loss dependencies are consistent with ionic conduction and Maxwell-Wagner-Sillars (MWS) polarisation processes [29]. Interestingly, dipole relaxation processes predominate at higher frequencies, whereas ionic conductivity appears to have a substantial role in G8's high loss values at lower frequencies.

### 4. CONCLUSION

A total of ten gallbladder samples were subjected to both qualitative and quantitative analyses to assess their composition. The results confirmed that the stones classified as Group I are primarily cholesterol stones, while those in Group II are comprised mainly of calcium carbonate. To identify the specific minerals present in these stones, X-ray diffraction (XRD) analysis was employed. This technique successfully identified cholesterol and bilirubin as the principal components, with the mineral identification being corroborated against the Joint Committee on Powder Diffraction Standards (JCPDS) files—specifically JCPDS 00-007-0742 for cholesterol and JCPDS 01-086-2343 for bilirubin. In addition to mineral characterization, dielectric spectroscopy was utilized to examine the interaction of gallbladder stones with electric fields. This advanced technique provides important insights into the electrical properties of the stones. Notably, the dielectric constant measured during the analysis indicates the stones' capacity to store electrical energy, which may have implications for understanding their behavior in various physiological and medical contexts.

### REFERENCE

- [1]. Selvaraju, R., Raman, R. G., Thiruppathi, G., & Valliappan, R. (2010). Epidemiological study of gallstone in Cuddalore District. *Int J Pharm Tech Res*, 2(2), 1061-1067.
- [2]. Shaffer, E. A. (2006). Epidemiology of gallbladder stone disease. *Best practice & research Clinical gastroenterology*, 20(6), 981-996.
- [3]. Shaffer, E. A. (1979). The role of the gallbladder in gallstone formation. In *Gallstones* (pp. 223-249). Boston, MA: Springer US.
- [4]. Patel, A. M., Yeola, M., Mahakalkar, C., Patel, A., & Mahakalkar, C. (2022). Demographic and risk factor profile in patients of gallstone disease in Central India. *Cureus*, *14*(5).
- [5]. Di Ciaula, A., Wang, D. Q. H., & Portincasa, P. (2018). An update on the pathogenesis of cholesterol gallstone disease. *Current opinion in gastroenterology*, 34(2), 71-80.
- [6]. Wilkins, T., Agabin, E., Varghese, J., & Talukder, A. (2017). Gallbladder dysfunction: cholecystitis, choledocholithiasis, cholangitis, and biliary dyskinesia. *Primary Care: Clinics in Office Practice*, 44(4), 575-597.
- [7]. Shaltout, A. A., Seoudi, R., Almalawi, D. R., Abdellatief, M., & Tanthanuch, W. (2024). Quantitative phase analysis and molecular structure of human gallstones using synchrotron radiation X-ray diffraction and FTIR spectroscopy. *Spectrochimica Acta Part A: Molecular and Biomolecular Spectroscopy*, 308, 123777.

- [8]. Liu, G., Xing, D., Wang, H., & Wu, J. (2002). Vibrational spectroscopic study of human pigment gallstones and their insoluble materials. *Journal of molecular structure*, 616(1-3), 187-191.
- [9]. Kleiner, O., Ramesh, J., Huleihel, M., Cohen, B., Kantarovich, K., Levi, C., & Mordechai, S. (2002). A comparative study of gallstones from children and adults using FTIR spectroscopy and fluorescence microscopy. *BMC gastroenterology*, 2(1), 3.
- [10]. Singh, V. K., Jaswal, B. S., Sharma, J., & Rai, P. K. (2020). Analysis of stones formed in the human gall bladder and kidney using advanced spectroscopic techniques. *Biophysical reviews*, *12*(3), 647-668.
- [11]. Gazali, Z., Gupta, V., Kumar, T., Kumar, R., Tarai, A. K., Rai, P. K., ... & Rai, A. K. (2023). Effect of mineral elements on the formation of gallbladder stones using spectroscopic techniques. *Analytical and Bioanalytical Chemistry*, 415(25), 6279-6289.
- [12]. Sharma, B., & Sharma, S. R. (2023). Microstructural and heavy metal analysis of gallstones prevalent in Jharkhand and its implications in the treatment. *Postgraduate Medicine*, *135*(3), 296-311.
- [13]. Salinas, G., Velásquez, C., Saavedra, L., Ramírez, E., Angulo, H., Tamayo, J. C., ... & Rodríguez, W. (2004). Prevalence and risk factors for gallstone disease. *Surgical Laparoscopy Endoscopy & Percutaneous Techniques*, 14(5), 250-253.
- [14]. Shabanzadeh, D. M. (2018). New determinants for gallstone disease. Dan Med J, 65(2), B5438.
- [15]. Dowais, R., Al Sharie, S., Araydah, M., Al Khasawneh, S., Haddad, F., & AlJaiuossi, A. (2021). Pearl-white gallstones: A report of a case and a chemical analysis by FTIR and XRD. *International Journal of Surgery Case Reports*, 87, 106449.
- [16]. Rautray, T. R., Vijayan, V., & Panigrahi, S. (2007). Analysis of Indian pigment gallstones. *Nuclear Instruments and Methods in Physics Research Section B: Beam Interactions with Materials and Atoms*, 255(2), 409-415.
- [17]. Malet, P. F., Takabayashi, A., Trotman, B. W., Soloway, R. D., & Weston, N. E. (1984). Black and brown pigment gallstones differ in microstructure and microcomposition. *Hepatology*, 4(2), 227-234.
- [18]. Abdallah, H. A. (2024). Endoscopic transpapillary gallbladder stenting for acute cholecystitis. *The Egyptian Journal of Surgery*, 43(2), 348-355.
- [19]. Raj, U., Kumar, A., & Mandial, V. (2022). Biochemical analysis of gallstones. *Int J Surg*, 6(1), 219-25.
- [20]. Arrout, A., El Ghallab, Y., Hirri, A., Aït Mouss, R., Yamari, I., Lefriyekh, M. R., ... & Said, A. A. H. (2024). Prediction of cholesterol content in gallstones by FTIR spectroscopy coupled with chemometric tools. *Microchemical Journal*, 199, 109956.
- [21]. Jayanthi, V., Sarika, S., Varghese, J., Vaithiswaran, V., Sharma, M., Reddy, M. S.& Kalkura, S. (2016). Composition of gallbladder bile in healthy individuals and patients with gallstone disease from north and South India. *Indian Journal of Gastroenterology*, 35(5), 347-353.
- [22]. Paluszkiewicz, C., Kwiatek, W. M., Gałka, M., Sobieraj, D., & Wentrup-Byrne, E. (1998). FT-Raman, FT-IR spectroscopy and PIXE analysis applied to gallstones specimens. *Cellular and Molecular Biology (Noisy-le-Grand, France)*, 44(1), 65-73.
- [23]. Zahra, A., ul Abadin, M. Z., Rahman, U. A., Changazi, S. H., Bhatti, S. U., Butt, U. I., & Iqbal, M. (2020). Morphological and Biochemical Analysis of Gallstones in Lahore, Pakistan. *Journal of Sheikh Zayed Medical College (JSZMC)*, 11(01), 12-16.
- [24]. Ali, S., Rasul, S., Dawani, S., Zahid, S., Hussain, S., Sarwar, O., ... & Tariq, Z. (2022). Effects of Chemical Composition of Cholesterol and Pigment Stones on the Gallbladder Mucosa. *Journal of Bahria University Medical and Dental College*, 12(02), 68-72.

- [25]. Ramya, J. Ramana, K. Thanigai Arul, M. Epple, U. Giebel, J. Guendel-Graber, V. Jayanthi, M. Sharma, M. Rela, and S. Narayana Kalkura. "Chemical and structural analysis of gallstones from the Indian subcontinent." *Materials Science and Engineering: C* 78 (2017): 878-885.
- [26]. Dawuti, W., Dou, J., Li, J., Liu, H., Zhao, H., Sun, L., ... & Lü, G. (2023). Rapid identification of benign gallbladder diseases using serum surface-enhanced raman spectroscopy combined with multivariate statistical analysis. *Diagnostics*, 13(4), 619.
- [27]. Prasad, K., Jha, A. K., & Chandra, K. P. (2008). Electrical properties of biogenic material: bilirubin rich gallstone. *International Journal of Nano and Biomaterials*, 1(3), 339-350.
- [28]. Singh, J., Bhatti, S. S., & Singh, V. R. (1995). Dielectric phase angle of gall stones as a function of density. *IEEE transactions on dielectrics and electrical insulation*, 2(6), 1159-1160.
- [29]. Rajan, R., Raj, N. A. N., Madeswaran, S., & Babu, D. R. (2015). Dielectric studies on struvite urinary crystals, a gateway to the new treatment modality for urolithiasis. *Spectrochimica Acta Part A: Molecular and Biomolecular Spectroscopy*, *148*, 266-270.